An Ion Balance for Ultra-High-Precision Atomic Mass Measurements

Simon Rainville, *et al.*

Science **303**, 334 (2004);
DOI: 10.1126/science.1092320

Science (print ISSN 0036-8075; online ISSN 1095-9203) is published weekly, except the last week in December, by the American Association for the Advancement of Science, 1200 New York Avenue NW, Washington, DC 20005.

RESEARCH ARTICLES

An Ion Balance for Ultra-High-Precision Atomic Mass Measurements

Simon Rainville,*† James K. Thompson, David E. Pritchard

We have developed the analog of a double-pan balance for determining the masses of single molecular ions from the ratio of their two cyclotron frequencies. By confining two different ions on the same magnetron orbit in a Penning trap, we balance out many sources of noise and error (such as fluctuations of the magnetic field). To minimize the systematic error associated with the Coulomb interaction between the two ions, they are kept about 1 millimeter apart from each other, resulting in fractional uncertainty below 1×10^{-11}. Such precision opens the door to numerous applications of mass spectrometry, including metrology, fundamental physics, and weighing chemical bonds.

Precise mass comparisons have wide-ranging applications in physics and metrology, including new determinations of the fine structure constant (*1*–*3*); a test of the fundamental charge, parity, and time reversal symmetry (*4*); understanding astrophysical heavy-element formation (*5*); a recalibration of the current γ-ray wavelength standard (*6*); and a possible route to realizing an atomic definition of the kilogram (*6*). In addition, the technique of ion cyclotron resonance used here is a very powerful tool in analytic and physical chemistry, allowing, for example, the determination of ion-molecule reaction pathways, kinetics, and equilibria in gas phase (*7*). Mass spectrometry is also being applied in a wide variety of areas, including protein structure, atmospheric chemistry, viral identification, forensics, and many others (*8*).

Besides their general value for metrology, improved mass comparisons with fractional accuracies of $\leq 10^{-11}$ can be used to test Einstein's mass-energy relationship $E = mc^2$ (*9*) and to help place limits on the electron neutrino rest mass (*10*). Our technique has already resulted in the measurement of the electric dipole moment of a charged molecule (*11*), providing a unique source of experimental data to physical chemists. Furthermore, it has the possibility of achieving accuracies of $\sim 10^{-12}$ in the future, which might allow the weighing of chemical binding energies of radicals that are too reactive or cannot be synthesized in large enough quantities for conventional laser spectroscopy.

Research Laboratory of Electronics, MIT-Harvard Center for Ultracold Atoms, and Department of Physics, Massachusetts Institute of Technology, Cambridge, MA 02139, USA.

*To whom correspondence should be addressed. E-mail: rainville@alum.mit.edu.

†Present address: Harvard University, 100 Edwin H. Land Boulevard, Cambridge, MA 02142, USA.

Measuring mass. The most precise mass measurements up to now were accomplished with the equivalent of a spring balance: by comparing the cyclotron frequencies of single ions alternately confined in a Penning trap, using either molecules (*1*, *6*) or highly charged ions (*12*–*14*). The precision was limited almost entirely by the variation of the magnetic field between the alternate measurements. Although such fluctuations can be virtually eliminated by carefully reducing and shielding magnetic field fluctuations (*12*), we have developed a technique to eliminate their effect. We simultaneously trap two different ions, allowing us to directly determine the difference between their cyclotron frequencies. This realizes the equivalent of a double-pan balance exhibiting large common mode rejection of many sources of noise and error besides magnetic field noise. We report here a mass comparison with this technique, obtaining a relative accuracy of 7×10^{-12}.

For this work, $^{13}C_2H_2^+$ and $^{14}N_2^+$ ions were used (ion 0 and ion 1, respectively), which constitute a "mass doublet" with very small mass difference, $\Delta m/m = 5.8 \times 10^{-4}$. The mass ratio $R = m_0/m_1$ is determined by measuring the ratio of the free space cyclotron frequencies f_{c0} and f_{c1}. Each f_{ci} is related to the mass by $2\pi f_{ci} = qB_0/m_i$, where B_0 is the magnetic field and q is the charge. A Penning trap is used to confine the ions in a small region of space (<1 mm^3) for several weeks, during which the mass ratio is repeatedly measured. The trap consists of an 8.5-T magnetic field and a set of rotationally symmetric hyperbolic electrodes, which are biased (~15 V) to provide confinement along the axial direction (*15*). For a single ion in the trap, the three normal modes and typical frequencies are the linear axial mode ($f_z \approx 200$ kHz) and the circular trap cyclotron ($f_{ct} \approx 5$ MHz) and magnetron modes ($f_m \simeq f_z^2/(2f_{ct}) \approx 5$ kHz).

Experimental overview. The basic idea of the two-ion technique described here is to arrange the ions on opposite sides of a shared circular magnetron orbit of diameter ~1 mm (Fig. 1A). The ions being ~1 mm apart from one another ensures that the ion-ion Coulomb interaction perturbs the measured cyclotron frequency ratio by less than 10^{-11}. Because the ions move on a shared magnetron orbit, they spatially average magnetic field inhomogeneities and electrostatic anharmonicities. This approach was investigated theoretically over 10 years ago (*15*).

By performing simultaneous cyclotron frequency comparisons in the same trap, we directly compare the cyclotron frequencies rather than using the magnetic field (and trap voltage) as an intermediate reference, as is done with alternating comparisons (*1*, *6*). The only quantity that must be measured precisely and accurately is the difference in trap cyclotron frequencies $f_{ct2} \equiv f_{ct1} - f_{ct0}$. The uncertainty on the cyclotron frequency ratio R is almost entirely determined by $\delta f_{ct2}/f_{ct2}$, but with roughly $m/\Delta m \sim 10^3$ more precision for a typical mass doublet. To calculate the cyclotron frequency ratio R to 10^{-11}, we need to obtain the trap cyclotron and axial frequencies of one of the ions (f_{ct0} and f_{z0}, or f_{ct1} and f_{z1}) with relative precision of only 10^{-8} and 10^{-5}, respectively (*15*, *16*), which reduces the requirements for the stability of the magnetic field and trap voltage by three orders of magnitude. Such relaxed requirements are currently met even during the daytime, when magnetic field fluctuations from nearby elevators and the Boston electric subway would prohibit performing alternating cyclotron frequency comparisons with precision below 10^{-9}. Also, f_{cti} and f_{zi} can be measured to much better than the required precision in a single 10-s measurement and would not be a limitation for mass comparisons at 10^{-12}.

To benefit from the common mode rejection of magnetic field and voltage noises (and for other reasons mentioned below), our two-ion technique can only be applied to mass doublets. But by using molecules containing hydrogen and deuterium, it is almost always possible to measure a particular atomic mass by comparing ions with $\Delta m/m \leq 10^{-3}$ (*17*).

Coupled magnetron motion. In our original proposal of the two-ion scheme (*15*), it was predicted that the small Coulomb interaction mixes the frequency-degenerate magnetron modes into two new collective modes: the common mode and the separation mode, with constant mode amplitudes ρ_{com} and ρ_s, respectively (Fig. 1B). The result that the ion-ion separation ρ_s is constant in time is crucial for accurately determining the mass

ratio, because most systematic errors vary strongly with ρ_s. The beat frequency Ω_m between the collective modes is given by

$$\Omega_m = \frac{q}{2\pi\epsilon_o B_0 \rho_s^3} \quad (1)$$

where ϵ_o is the electric constant. At an ion-ion separation of $\rho_s = 1$ mm, the beat frequency is $\Omega_m = 2\pi \times 54$ mHz. The beating of the collective modes manifests itself as a slow modulation of each ion's instantaneous magnetron amplitude ρ_{mi} that proves the key to observing and controlling the collective magnetron motion.

To load a pair of dissimilar ions into the trap, we first create a single $^{13}C_2H_2^+$ ion from $^{13}C_2H_2$ gas by electron impact ionization. The electron beam is produced by a field emission point and is nearly coaxial with the trap, so the ion is created with a small magnetron radius ($\leq$100 μm). Unwanted ions are removed using our standard cleaning techniques (*15*). The first ion is then driven into a large magnetron orbit of radius $\rho_{m0} = 1$ mm, and a single $^{14}N_2^+$ ion is created near the center of the trap from $^{14}N_2$ gas. The magnetron modes immediately couple, and the common and separation amplitudes are given by $\rho_s = 2\rho_{com} = \rho_{m0} = 1$ mm.

Observing the magnetron motion. In order to observe and control the relative magnetron motion, we use small imperfections in the Penning trap electrostatic and magnetic fields. The imperfections cause each mode frequency f_{ct}, f_z, and f_m to slightly vary with the three mode amplitudes ρ_c, z, and ρ_m. The Penning trap magnetic and electrostatic fields can be described by multipole expansions about the center of the trap with expansion coefficients B_n and C_n, respectively, using the conventions of (*18*). Because the ions are not at the center of the trap, their motions are sensitive to B_2, B_4, C_4, and C_6. The electrostatic anharmonicity C_4 can be quickly varied under computer control (in ~20 ms) (*19*).

To determine the ion-ion separation ρ_s, the beat frequency Ω_m between the collective magnetron modes is measured. The beat frequency must be determined from the axial motion of each ion, the only mode that is directly detected and damped (*20*). To do so, we deliberately distort the trap potential with a nonzero C_4 so that when $\rho_{com} \neq 0$, the modulation of the magnetron radius at Ω_m causes a modulation of the axial frequency, also at Ω_m. The instantaneous axial frequency of one ion is monitored with a phase-locked feedback system. From the observed frequency modulation, the ion-ion separation can be determined to ~1% (in ~100 s). Because of the electrostatic anharmonicity and finite axial amplitude used to perform the measurement, a 5% uncertainty is assigned to our measurement of ρ_s. The common mode amplitude ρ_{com} can be determined to 25% from the amplitude of the axial frequency modulation and knowledge of the electrostatic anharmonicity.

Controlling the magnetron motion. Now that ρ_{com} can be measured, we need to set it to zero to place the ion pair on the desired magnetron orbit (Fig. 1A). This is enabled by a nonlinear coupling technique that resonantly and reversibly transfers canonical angular momentum between the common and separation magnetron modes (*21*). The coupling is nonlinear in the amplitudes ρ_s and ρ_{com}, because it is driven by the modulation of the radial position of the ions, which goes to zero as ρ_{com} goes to zero. As a result, the system will exponentially relax

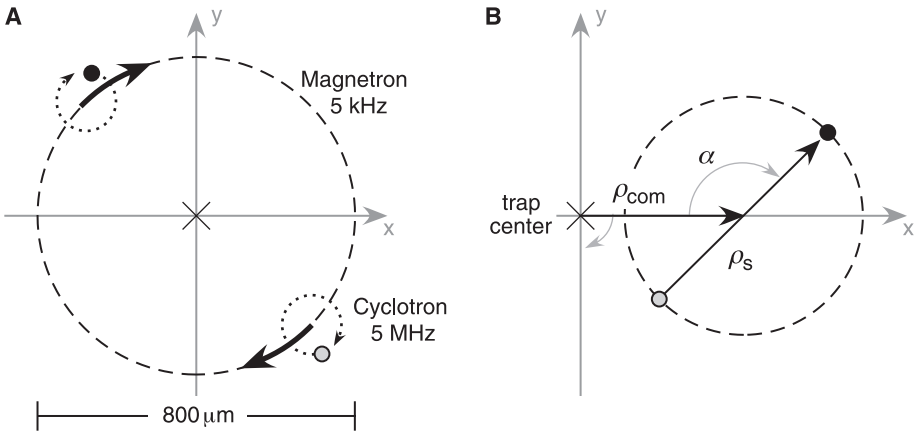

Fig. 1. The dynamics of the strongly coupled magnetron modes. The diagrams depict the orbits of the ions in the radial plane, with the magnetic field pointing out of the page. (**A**) The ideal configuration for taking precise mass measurements. The two different ions orbit the trap center (cross) on a shared magnetron orbit ~800 μm in diameter. To perform the cyclotron frequency comparison, small (~150 μm in diameter) cyclotron orbits (small dashed circles) are superposed on top of the larger magnetron motion. The ideal shared magnetron orbit is a special case ($\rho_{com} = 0$) of the more general collective magnetron motion that is shown in (**B**), without the cyclotron motion for simplicity. The Coulomb interaction mixes the frequency-degenerate magnetron modes into two new collective modes: the common mode and the separation mode, with definitions $\vec{\rho}_{com} = (\vec{\rho}_{m1} + \vec{\rho}_{m0})/2$ and $\vec{\rho}_s = (\vec{\rho}_{m1} - \vec{\rho}_{m0})$. The common mode corresponds to the center of charge orbiting the electrostatic center of the trap at the average magnetron frequency. In a rotating frame where $\vec{\rho}_{com}$ is fixed, the ions execute a stable $E_{ion-ion} \times B_0$ drift about the center of charge (dashed circle), so that the angle between the vectors $\vec{\rho}_s$ and $\vec{\rho}_{com}$ varies as $\alpha = \Omega_m t$. We have developed techniques to set $\rho_{com} = 0$ and to measure and control ρ_s.

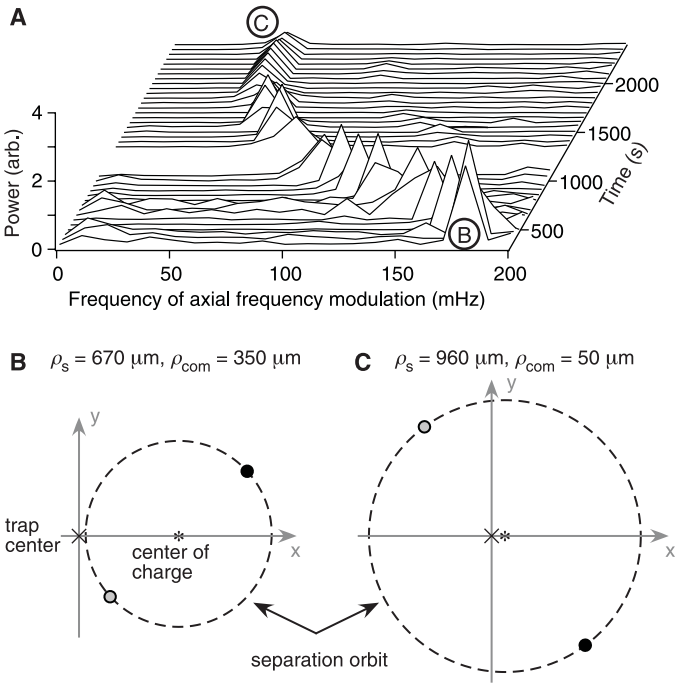

Fig. 2. Transferring canonical angular momentum from the collective magnetron common mode to the collective separation mode. In (**A**), power spectra of the instantaneous axial frequency of ion 0 are shown for a sliding time window of 100 s centered at "Time." The magnetron beat frequency Ω_m (and hence the ion-ion separation ρ_s) is determined from the frequency of the peak. By placing a constant axial drive below the axial resonance and introducing an electrostatic anharmonicity C_4, canonical angular momentum in the common mode can be transfered to the separation mode, causing the ion-ion separation ρ_s to increase and Ω_m to decrease, until $\rho_{com} \approx 0$. The initial magnetron motion is shown in (**B**), and the final magnetron motion, which approximates the ideal parked orbit configuration of Fig. 1A, is shown in (**C**).

to the desired configuration with $\rho_{com} = 0$.

The coupling starts with a fixed-frequency axial drive applied just below the axial resonance of one of the ions. In the presence of electrostatic anharmonicities, the detuning of the axial frequency of the ion from the fixed frequency drive is modulated at the beat frequency Ω_m because of the changing radial position in the trap. Thus, the axial frequency modulation is converted into axial amplitude modulation. The axial amplitude modulation combined with the electrostatic anharmonicity generates a modulation of the instantaneous magnetron frequency of that ion. Because of the finite response time of the axial mode ($\tau \sim 1$ s), the magnetron frequency modulation lags the axial amplitude modulation by approximately $2\Omega_m\tau \sim \pi/10$, which is important for establishing the desired phase relationship. As the ions pass through equal magnetron radii, the lagging magnetron frequency modulation of the driven ion creates a small phase advance or lag of its magnetron position with respect to the other ion (as measured from the center of the trap). This magnetron phase advance or lag is modulated at Ω_m, so that the relative phase shifts coherently add. The result is that the ions slowly "walk" away from one another; that is, ρ_s increases. Because no torque is applied in the process, the canonical angular momentum, which is roughly proportional to $\rho_{com}^2 + \rho_s^2/4$, is conserved, and ρ_{com} decreases (*22*). Figure 2 illustrates this nonlinear coupling in action by showing the evolution of the measured beat frequency Ω_m toward an asymptote with $\rho_{com} = 0$.

Using this collective magnetron coupling technique, the canonical angular momentum in the common mode can be moved into the separation mode, so that the common mode amplitude is typically $\rho_{com} \leq 0.05 \times \rho_s$ (*23*). The minimum value of ρ_{com} is limited by detection noise and nonadiabatic variation of axial amplitudes and trap anharmoncities with respect to the time scale set by the beat frequency between the modes Ω_m. We have been able to experimentally verify that when the ions are in this ideal configuration, the phases of their magnetron motions differ by 180° ± 10° and that the root mean square (RMS) magnetron radii of the ions are equal to $\rho_s/2$ within the error. These are further independent empirical confirmations that our model of collective magnetron motion is correct even in a slightly imperfect Penning trap (*21*).

The collective magnetron mode coupling technique allows us to systematically vary the ion-ion separation. To increase ρ_s, we first set $\rho_{com} \approx 0$ and then inject angular momentum into the common mode with a resonant dipole drive that acts symmetrically on both magnetron modes, leaving ρ_s unchanged but setting $\rho_{com} \approx 300$ μm. The injected angular momentum can then be transfered into the separation mode with our coupling technique, thus reducing ρ_{com} and making ρ_s larger. To move the ions closer together, angular momentum is removed from the system by simultaneously applying brief resonant sideband couplings between each ion's individual magnetron mode and its damped axial mode.

The ideal magnetron configuration ($\rho_{com} \approx 0$) was found to be extremely stable in time. No change in ρ_s or ρ_{com} was observed when the ions were left in the trap for many days with thermal (4 K) axial motion. When performing cyclotron frequency comparisons, during which the cyclotron and axial modes were excited, ρ_s and ρ_{com} were observed to slowly change in a manner consistent with the total canonical angular momentum in the magnetron modes remaining constant. For scale, ρ_{com} would often change by ~100 μm over 5 hours. This change can be described as a random diffusion of canonical angular momentum between the collective modes. The diffusion is driven by an interaction analogous to our collective magnetron coupling technique, except that here the axial modes are briefly excited at random times with respect to the relative phase of the collective magnetron modes. The cyclotron frequency comparisons were typically paused for 20 min every 5 to 10 hours to measure ρ_s and reset ρ_{com} to zero.

Measuring the mass ratio. Once the ions are located on a shared magnetron orbit, their cyclotron frequencies can be simultaneously measured using our pulse and phase (PNP) technique (*24*). The PNP technique is based on measuring the amount of cyclotron phase accumulated after some evolution time T_{evol} (varying from 0.1 s to over 10 min) during which the cyclotron modes are undetected and undamped. The cyclotron phase measurement is accomplished using a radio frequency coupling pulse (π pulse) to map the cyclotron phase at the end of the evolution time onto the detected axial mode (Fig. 3A). Figure 3B shows the cyclotron phase of ion 1 versus ion 0 after simultaneously accu-

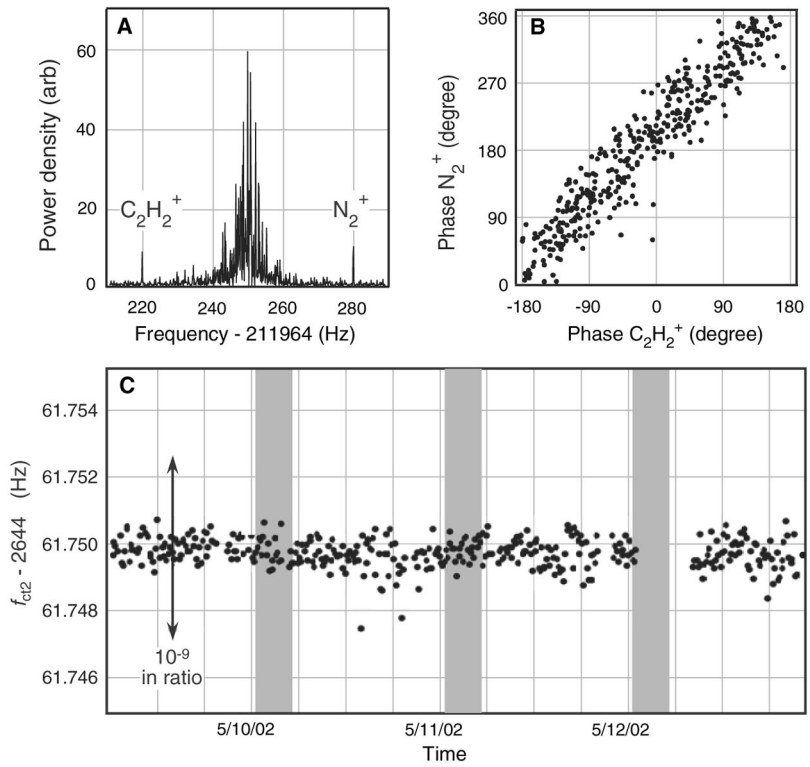

Fig. 3. Data demonstrating the two-ion technique. (**A**) Power spectrum of the current induced in our detector by the axial motions of the ions, recorded for 8 s. The axial signals of the two ions are 31 Hz above and below the resonance frequency of the detection circuit and can be observed simultaneously. The Lorentzian profile of the 4.2 K Johnson noise is visible in the middle. In (**B**), the measured phase of ion 1's axial signal is plotted against the phase of ion 0, obtained after repeated PNPs with $T_{evol} = 200$ s. The strong correlation between the phases shows the common mode rejection of magnetic field and trap voltage noise in this technique, resulting in a large gain in precision. From the difference between these phases, we obtain the crucial trap cyclotron frequency difference f_{ct2}, which is plotted versus time in (**C**). The standard deviation of the measurements is $\sigma f_{ct2}/f_{ct1} = 7 \times 10^{-11}$, leading to a measurement of the mass ratio of 1×10^{-11} in only 5 hours. For scale, a variation of the size indicated by the vertical arrow would correspond to a fractional variation of 10^{-9} in the ratio. The gray bands indicate the time windows during which the absence of magnetic field noise from the Boston subway would have allowed cyclotron frequency comparisons if the previous alternating technique had been used.

mulating cyclotron phases for T_{evol} = 200 s. Magnetic field variation causes the phases to vary over 2π, but the phases are well correlated with each other because the ions experienced the same magnetic and trap voltage noise during T_{evol}. In fact, the two cyclotron modes have been allowed to simultaneously evolve phase for as long as T_{evol} = 30 min without losing a single cycle in the relative cyclotron motions of the ions.

The crucial trap cyclotron frequency difference f_{ct2} versus time is shown in Fig. 3C. The standard deviation of the measurements $\sigma f_{ct2}/f_{ct1}$ is 7×10^{-11}. Typically, the cyclotron frequency ratio can be measured to a precision of 10^{-11} in only 5 hours of data taking. The ability to take data 24 hours a day (almost completely under computer control) also increases the amount of data that can be taken by a factor of 5.

Sources of error and limitations. There are two significant sources of systematic error in this technique: Coulomb interactions between the ions and trap field imperfections (e.g., B_2, B_4, C_4, and C_6). Our chief concern is with systematic perturbations of the trap cyclotron frequency difference f_{ct2} (*25*).

The largest potential source of systematic error arising from ion-ion interactions results from a possible asymmetry in the cyclotron radii of the two ions (*15*). The magnitude of this shift has been experimentally confirmed by purposely setting the imbalance between the cyclotron amplitudes to a large value of 20% (ρ_{c1}/ρ_{c0} = 1.2). This caused f_{ct2} to change by $\Delta f_{ct2}/f_{ct1} = 50(10) \times 10^{-12}$ at ρ_s = 700 μm, in agreement with the predicted value (to within errors) (*26*). When taking precise mass comparison data, we obviously strive to make the cyclotron radii equal to each other, and we experimentally put an upper limit of 2.6% on the imbalance in this case (*16*). This uncertainty translates into an upper limit of 4×10^{-12} for the potential systematic error on the ratio at ρ_s = 750 μm, and decreases as ρ_s^{-5} for larger separations.

The measurement of the trap cyclotron frequency difference is slightly sensitive to radially dependent trap field imperfections. The small difference in centrifugal force leads to a slight imbalance in the magnetron radii of the two ions parameterized as $\vec{\rho}_{m1} = \vec{\rho}_s(1 - \delta_{mag})/2$ and $\vec{\rho}_{m0} = -\vec{\rho}_s(1 + \delta_{mag})/2$ with $\delta_{mag} = (4\pi^3\epsilon_o)\Delta m f_m^2 \rho_s^3/q^2$. For $^{13}C_2H_2^+$ and $^{14}N_2^+$, δ_{mag} = 0.027 at ρ_s = 1 mm. The predicted imbalance in the RMS magnetron radii was experimentally confirmed to 30% (over ion-ion separations ρ_s = 700 to 1100 μm) from measurements of the trap cyclotron frequency difference f_{ct2} versus C_4.

To minimize the systematic error due to radially dependent trap field imperfections, we first carefully measure B_2, B_4, C_6, and the ion-ion separation ρ_s. We can then adjust C_4 to create an extreme in the function of trap cyclotron frequency shift versus magnetron radius at the average magnetron radius of the two ions; that is, $\rho_m = \rho_s/2$. At this "optimal C_4," the measurement of the trap cyclotron frequency difference f_{ct2} is only sensitive to trap imperfections at order δ^3_{mag}. Measurement of the trap cyclotron frequency difference can be optimized using C_4, because we do not need to measure the individual trap cyclotron or axial frequencies very accurately. Uncertainties in B_2, B_4, C_4, C_6 (*19*), and the ion-ion separation ρ_s (~5%) translate into an upper limit of 4×10^{-12} for the possible uncanceled systematic error at a separation of 750 μm.

Results. The above estimates of systematic errors can be tested by measuring the cyclotron frequency ratio versus ion-ion separation. The data (Fig. 4) provide strong evidence that the systematic errors have been overestimated, because the measured ratio varies by much less than predicted from our estimates (*27*). Nonetheless, we conservatively rely on the above estimates of systematic errors to obtain a 1σ confidence interval uncertainty of 7×10^{-12} for the following mass ratio (*28*)

$$R = \frac{m[^{14}N_2^+]}{m[^{13}C_2H_2^+]} = 0.999\,421\,460\,888\,(7) \qquad (2)$$

Without loss of precision, we can express the above result as a difference of neutral masses (in atomic units, u) by accounting for the mass of the missing electrons and chemical binding energies (*16*, *29*, *30*)

$$M[^{13}C] + M[H] - M[^{14}N] = 0.008\,105\,862\,88\,(10)\ \text{u} \qquad (3)$$

Results with comparable accuracy have been obtained (with a different setup) by taking extreme precautions to stabilize the magnetic field while making alternating measurements on multiply ionized atoms over several months (*12*, *31*). A number of other labs have recently achieved results with accuracies between a few parts in 10^{10} and 10^9 (*13*, *14*).

Outlook. The precision of our method is limited by cyclotron frequency noise arising from thermal fluctuations in the cyclotron amplitudes, coupled to relativistic shifts and nonlinear ion-ion interactions. We have previously demonstrated that the amplitude fluctuations can be reduced using squeezing (*32*) or electronic refrigeration techniques (*33*). Systematic errors can be reduced and further checked by using nonresonant sideband couplings to reduce the magnetron imbalance δ_{mag} by an order of magnitude (*21*); randomizing the roles of the two cyclotron drive synthesizers to reduce possible cyclotron radius imbalance by an order of magnitude; and measuring the same mass ratio at different mass-to-charge ratios; for example, comparing $^{13}C_2H_2^+$ versus $^{14}N_2^+$ to $^{13}CH^+$ versus $^{14}N^+$. Thus, our method of directly comparing the cyclotron frequencies of two ions, with its high precision and common mode

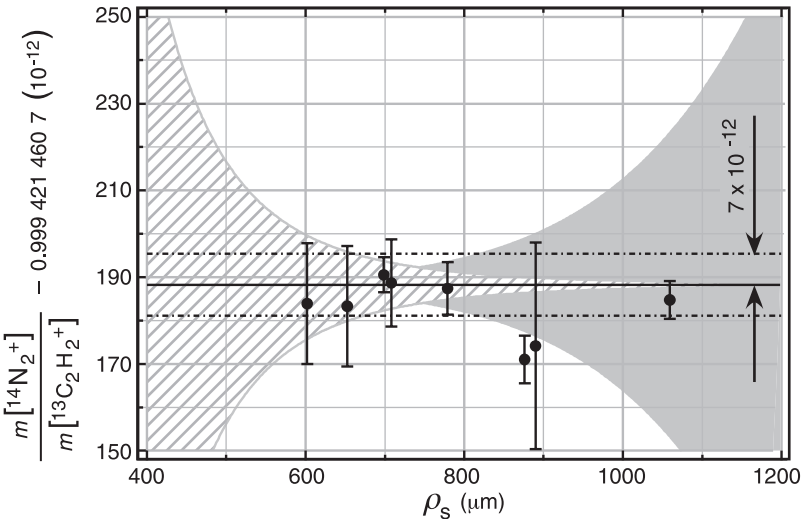

Fig. 4. The measured mass ratio as a function of ion-ion separation distance ρ_s. The bands show the upper limits on the systematic errors from ion-ion interactions (hatched area) and trap field imperfections (gray area). Both uncertainties scale very strongly with ion-ion separation [at a minimum as ρ_s^{-5} and ρ_s^5, respectively (*15*)] so that even though we have changed ρ_s by only a factor of 1.8, the systematic errors have changed by at least a factor of 20, going from the smallest to the largest separation. The fact that all our data points lie within 2×10^{-11} of each other shows that we have been very conservative in our estimate of systematic errors. The solid line shows our best estimate of the mass ratio with a total 1σ confidence interval uncertainty of 7×10^{-12} (dashed horizontal lines). The contributions to this error from statistics, trap imperfection, and ion-ion interactions are 3.0×10^{-12}, 3.4×10^{-12}, and 5.5×10^{-12}, respectively.

rejection of many sources of noise and error, should hold promise for ultimately accomplishing mass comparisons at 1×10^{-12} or 2×10^{-12}. For a molecule with mass 30 u, such precision would provide an energy resolution of 0.03 eV, allowing direct weighing of chemical binding energies to a few percent. This would be a new tool to investigate simple ionic species not amenable to conventional spectroscopic and thermochemical techniques.

References and Notes

1. M. P. Bradley, J. V. Porto, S. Rainville, J. K. Thompson, D. E. Pritchard, *Phys. Rev. Lett.* **83**, 4510 (1999).
2. A. Wicht, J. M. Hensley, E. Sarajlic, S. Chu, *Phys. Scr.* **T102**, 82 (2002).
3. E. Kruger, W. Nistler, W. Weirauch, *Metrologia* **35**, 203 (1998).
4. G. Gabrielse *et al.*, *Phys. Rev. Lett.* **82**, 3198 (1999).
5. B. Fogelberg, K. A. Mezilev, H. Mach, V. I. Isakov, J. Slivova, *Phys. Rev. Lett.* **82**, 1823 (1999).
6. F. DiFilippo, V. Natarajan, K. R. Boyce, D. E. Pritchard, *Phys. Rev. Lett.* **73**, 1481 (1994).
7. A. Marshall, C. L. Hendrickson, G. S. Jackson, *Mass Spectrom. Rev.* **17**, 1 (1998).
8. G. Siuzdak, *The Expanding Role of Mass Spectrometry in Biotechnology* (MCC Press, San Diego, CA, 2003).
9. G. L. Greene, M. S. Dewey, E. G. Kessler, E. Fischbach, *Phys. Rev. D* **44**, R2216 (1991).
10. V. M. Lobashev, *Nucl. Phys. A* **A719**, 153c (2003).
11. J. K. Thompson, S. Rainville, D. E. Pritchard, in preparation.
12. R. S. Van Dyck, D. L. Farnham, S. L. Zafonte, P. B. Schwinberg, *Rev. Sci. Instrum.* **70**, 1665 (1999).
13. I. Bergstrom *et al.*, *Nucl. Instrum. Methods A* **487**, 618 (2002).
14. T. Beier *et al.*, *Phys. Rev. Lett.* **88**, 011603 (2002).
15. E. A. Cornell, K. R. Boyce, D. L. K. Fygenson, D. E. Pritchard, *Phys. Rev. A* **45**, 3049 (1992).
16. S. Rainville, thesis, Massachusetts Institute of Technology, Cambridge, MA (2003).
17. Measured molecular binding energies are used to determine the atomic mass of neutral atoms from our measured molecular mass ratios. The uncertainty on the molecular binding energies only limits the accuracy of the neutral atomic mass to a few parts in 10^{12}, because for most molecules, the binding energies typically represent a correction of a few parts in 10^{10}, and they are known to better than a few percent. For molecules with poorly measured binding energies, mass comparisons can be used to directly weigh the chemical binding energy, as discussed in the text.
18. L. S. Brown, G. Gabrielse, *Rev. Mod. Phys.* **58**, 233 (1986).
19. The measured magnetic field inhomogeneities after shimming are $B_2 = 6.1(6) \times 10^{-9} B_0/\mathrm{mm}^2$ and $B_4 = 1.2(5) \times 10^{-9} B_0/\mathrm{mm}^4$, where $B_0 = 8.53$ T. The measured electrostatic anharmonicity is $C_6 = 0.0011(1)$. The value of C_4 is varied using the guard ring electrodes located between the endcap and the ring electrodes. The C_4 was purposely set to values of $|C_4| \leq 1.5 \times 10^{-4}$ for reasons described in the text, but could be zeroed to $\pm 4 \times 10^{-6}$ if desired.
20. For phase-sensitive detection of the axial mode, the image currents that each ion's axial motion induces across the trap electrodes are coupled to a dc superconducting quantum interference device via a superconducting self-resonant transformer (with a quality factor of about 47,000).
21. J. K. Thompson, thesis, Massachusetts Institute of Technology, Cambridge, MA (2003).
22. The canonical angular momentum can also be transferred from the separation mode to the common mode by placing the fixed axial drive above the axial resonance, thereby changing the phase of the magnetron frequency modulation by π and making ρ_s decrease while ρ_{com} increases.
23. Even if the common mode amplitude is not precisely zeroed, the beating of the two collective modes will lead to time averaging of the radially dependent magnetic field inhomogeneities on a time scale much shorter than the one needed for a typical cyclotron frequency comparison.
24. E. A. Cornell, R. M. Weisskoff, K. R. Boyce, D. E. Pritchard, *Phys. Rev. A* **41**, 312 (1990).
25. Only at the smallest ion-ion separations of $\rho_s \leq 500$ μm is the perturbation of the measured axial frequency significant enough to affect the measured cyclotron frequency ratio at 10^{-11}.
26. The sign of the originally predicted shift [eq. 4-14 in (*15*)] was found to be incorrect.
27. The measured ratio has not shown any systematic variation with ρ_s either in three preliminary data sets using different molecules.
28. There is no polarization shift of the cyclotron frequency of $^{13}C_2H_2^+$ at the current level of precision, because the ion has zero effective dipole moment in its linear electronic ground state (*11*, *34*).
29. M. W. Chase, *J. Phys. Chem. Ref. Data* **9**, 1 (1998).
30. P. Linstrom, W. Mallard, Eds., NIST Chemistry WebBook, NIST Standard Reference Database Number 69, March 2003 Release (National Institute of Standards and Technology, Gaithersburg, MD, 20899) (http://webbook.nist.gov).
31. R. S. VanDyck, S. L. Zafonte, P. B. Schwinberg, *Hyperfine Interact.* **132**, 163 (2001).
32. V. Natarajan, F. DiFilippo, D. E. Pritchard, *Phys. Rev. Lett.* **74**, 2855 (1995).
33. S. Rainville, M. P. Bradley, J. V. Porto, J. K. Thompson, D. E. Pritchard, *Hyperfine Interact.* **132**, 177 (2001).
34. M. F. Jagod *et al.*, *J. Chem. Phys.* **97**, 7111 (1992).

35. We acknowledge with gratitude that the experimental and measurement technologies that have made these experiments possible are the result of about 20 years of effort by previous group members, especially the detector technology developed by M. P. Bradley and J. V. Porto. We thank E. G. Myers for many helpful comments on the manuscript. This work was supported by NSF and was formerly supported by the National Institute of Science and Technology and the Joint Services Electronics Program. S.R. acknowledges the support of the Fonds pour la Formation de Chercheur et l'Aide à la Recherche.

7 October 2003; accepted 18 November 2003
Published online 11 December 2003;
10.1126/science.1092320
Include this information when citing this paper.

Finite-Frequency Tomography Reveals a Variety of Plumes in the Mantle

Raffaella Montelli,[1]* Guust Nolet,[1] F. A. Dahlen,[1] Guy Masters,[2] E. Robert Engdahl,[3] Shu-Huei Hung[4]

We present tomographic evidence for the existence of deep-mantle thermal convection plumes. *P*-wave velocity images show at least six well-resolved plumes that extend into the lowermost mantle: Ascension, Azores, Canary, Easter, Samoa, and Tahiti. Other less well-resolved plumes, including Hawaii, may also reach the lowermost mantle. We also see several plumes that are mostly confined to the upper mantle, suggesting that convection may be partially separated into two depth regimes. All of the observed plumes have diameters of several hundred kilometers, indicating that plumes convey a substantial fraction of the internal heat escaping from Earth.

Hotspots are characterized by higher temperature, topographic swells, and recent volcanism with isotopic signatures distinct from those that characterize mid-ocean ridge or andesitic basalts (*1*–*3*). The best known example is the Hawaii-Emperor volcanic chain, which may have formed as the Pacific plate moved over a deep magmatic source (*3*–*10*). Narrow thermal upwellings in the form of plumes are commonly observed in laboratory experiments (*11*, *12*) and numerical simulations (*13*–*15*), and deep-mantle plumes have been invoked to explain flood basalts, the isotopic signature of ocean island basalts, and the topography of the swells and plateaus that often accompany volcanic hotspots. Although this has led to a coherent (albeit incomplete) theory of much of the geology that characterizes hotspots, undisputed evidence for the existence of lower-mantle plumes in tomographic images of the mantle is lacking. High temperatures reduce the velocity of seismic waves, so that plumes should be evinced as columnar low-velocity anomalies. In the absence of convincing tomographic evidence, it has recently been argued that hotspots could instead be the manifestation of shallow, plate-related stresses that would fracture the lithosphere, causing volcanism to occur along these cracks (*16*–*18*).

The inversion. A unique feature of our tomographic inversion is the use of finite-frequency sensitivity kernels (*19*, *20*) to account for effects of wavefront healing on the travel times of low-frequency *P* waves; this enables us to combine long- and short-period data sets. We use a remeasured, expanded set of long-period data and very carefully selected short-period delay times, and we adapt the model parameterization to the lower resolution at depth. Global

[1]Department of Geosciences, Princeton University, Princeton, NJ 08544, USA. [2]Institute of Geophysics and Planetary Physics, University of California at San Diego, La Jolla, CA 92093, USA. [3]Department of Physics, University of Colorado, Boulder, CO 80309, USA. [4]Department of Geosciences, National Taiwan University, Taipei, Taiwan.

*To whom correspondence should be addressed. E-mail: montelli@princeton.edu